# Deciphering the Role of Individual Acyl Chains in the Interaction Network between Phosphatidylserines and a Single-Spanning Membrane Protein†

Florence Mousson,‡ Yves-Marie Coïc,§ Françoise Baleux,§ Veronica Beswick,‡,|| Alain Sanson,‡,|| and Jean-Michel Neumann*,‡

*Service de Biophysique des Fonctions Membranaires, CEA DSV/DBJC and URA CNRS 2096, Centre d'Etudes de Saclay, 91191 Gif sur Yvette Cedex, France, Unité de Chimie Organique, URA CNRS 487, Institut Pasteur, 28 rue du Dr Roux, 75724 Paris Cedex, France, Université d'Evry, Bd F. Mitterrand, 91025 Evry, France, and Université Pierre et Marie Curie, 9 quai Saint-Bernard, Bât C, 75005 Paris, France*

*Received June 10, 2002; Revised Manuscript Received September 14, 2002*

ABSTRACT: PMP1 is a small single-spanning membrane protein functioning as a regulatory subunit of the yeast plasma membrane $H^+$-ATPase. This protein forms a unique helix and exhibits a positively charged cytoplasmic domain that is able to specifically segregate phosphatidylserines (PSs). A marked groove formed at the helix surface is thought to play a major role in the related lipid−protein interaction network. Mutational analysis and $^1$H NMR experiments were therefore performed on a synthetic PMP1 fragment using DPC-$d_{38}$ micelles as a membrane-like environment, in the presence of small amounts of POPS. A mutation designed for altering the helix groove was shown to disfavor the POPS binding specificity as much as that affecting the electrostatic interaction network. From POPS titration experiments monitored by a full set of one- and two-dimensional NOESY spectra, the association between the phospholipids and the PMP1 peptide has been followed. Our data reveal that the clustering of POPS molecules is promoted from a stabilized framework obtained by coupling the PMP1 helix groove to a POPS *sn*-2 chain. To our knowledge, the NOE-based titration plots displayed in this report constitute the first NMR data that directly distinguish the role of the *sn*-1 and *sn*-2 acyl chains in a lipid−protein interaction. The results are discussed while taking into account our accurate knowledge of the yeast plasma membrane composition and its ability to form functional lipid rafts.

Over the past few years, the amount of crystallographic data elucidating membrane protein structures has spectacularly increased (*1*−*9*), while in parallel, the contribution of NMR[1] spectroscopy in this field appears to be more and more successful (*10*−*16*). Combined with meaningful results obtained from model peptides (*17*−*22*), all these studies progressively reveal general features characterizing the structural properties of membrane proteins. In contrast, and despite early efforts, the molecular basis underlying lipid−protein interactions and especially their specificity remain poorly understood (*23*, *24*). It is however clear that elucidating the interaction network driving specific association between lipids and membrane proteins would be essential for a better understanding of their sequence−structure−function relationships. Furthermore, such data are very much needed taking into account our increasing knowledge of membrane functional organization as judged by the growing number of reports devoted to microdomains and lipid rafts (*25*−*31*, and references therein).

In this context, we focus on the structural and lipid binding properties of the membrane protein PMP1, a regulatory subunit of the yeast plasma membrane $H^+$-ATPase (*32*, *33*). This protein offers several advantages that are summarized as follows.

(i) PMP1 is a small single-spanning membrane protein that is well-adapted to NMR studies in micelles; its sequence ($L_1$-P-G-G-$V_5$-I-L-V-F-$I_{10}$-L-V-G-L-$A_{15}$-C-I-A-I-$I_{20}$-A-T-I-I-**$Y_{25}$-R-K-W-Q-$A_{30}$-R-Q-R-G-$L_{35}$-Q-R-$F_{38}$**) exhibits a positively charged cytoplasmic domain at its C-terminus (bold residues) but no polar residue at its N-terminus.

(ii) PMP1 belongs to the proteolipid family, sharing with the lipids the common property of being soluble in chloroform/methanol media.

(iii) The endogenous lipid environment of PMP1, i.e., that of the yeast plasma membrane, is accurately known (*34*); in particular, it exhibits an outer leaflet enriched in sphingolipids forming rafts (*35*) and an inner leaflet containing most of the PS lipids, mainly the monounsaturated POPS species.

The conformational properties of several synthetic fragments of PMP1, solubilized in DPC-$d_{38}$ micelles, were

† The 800 MHz spectra were recorded on the spectrometer installed at ICSN-CNRS, procured with the help of the Région Ile de France and the Association pour la Recherche contre le Cancer.

* To whom correspondence should be addressed. Fax: 33 1 69 08 81 39. E-mail: neumann@dsvidf.cea.fr.

‡ Centre d'Etudes de Saclay.

§ Institut Pasteur.

|| Université d'Evry and Université Pierre et Marie Curie.

[1] Abbreviations: DIPEA, *N*,*N*-diisopropylethylamine; DPC, dodecylphosphocholine; DSS, 2,2-dimethyl-2-silapentane-5-sulfonate; EDT, 1,2-ethanedithiol; HATU, *O*-(7-azabenzotriazol-1-yl)-1,1,3,3-tetramethyluronium hexafluorophosphate; MPLC, medium-pressure liquid chromatography; NMR, nuclear magnetic resonance; NOESY, nuclear Overhauser enhancement spectroscopy; POPC, 1-palmitoyl-2-oleoyl-3-glycerophosphatidylcholine; POPS, 1-palmitoyl-2-oleoyl-3-glycerophosphatidylserine; PS, phosphatidylserine; TFA, trifluoroacetic acid; TIS, triisopropylsilane; TOCSY, total correlated spectroscopy.

10.1021/bi026274b CCC: $22.00 © 2002 American Chemical Society
Published on Web 10/23/2002

studied by $^1$H NMR (*36*−*38*). The fragments correspond to the A18−F38, G13−F38, and F9−F38 peptides, the latter spanning 80% of the whole sequence. In all cases, a single helix conformation extending from the N-terminus up to Q32 was found. The C-terminal extremity, R33−F38, folds back toward the micelle interior (*39*). As a result, the PMP1 cytoplasmic domain exhibits a ring-like interfacial distribution of five basic side chains and has been shown by $^2$H NMR to specifically segregate POPS molecules when inserted in mixed POPC/POPS bilayers (*40*). In parallel, mutational analyses associated with $^1$H NMR experiments (*37*) were performed on the G13−F38 peptide solubilized in DPC-$d_{38}$ micelles in the presence of small amounts of either POPC or POPS lipids ([POPX]/[peptide] ∼ 4). The major finding of our mutational study was the concerted influence of residues W28 and Q32 on both the helix conformation and the POPS binding specificity of PMP1 at the membrane interface.

The aim of this study is to investigate the hydrophobic aspect of PMP1−POPS binding in an effort to further decipher what is thought to be a fine-tuned electrostatic and hydrophobic interaction network adapted to the yeast plasma membrane environment. As illustrated in Figure 1, the observation underlying our prospect is the occurrence of a groove formed at the PMP1 helix surface by the ($i$, $i$ + 3) distribution of alanine residues (A15, A18, and A21) in an isoleucine-rich region (I17, I19, I20, I23, and I24). One can notice that (i) two aromatic side chains, Y25 and W28, border the entry site of the "alanine" groove and (ii) the groove approximately spans a standard hydrophobic domain of only one membrane leaflet. Simple molecular modeling readily indicates that an acyl chain of a phospholipid molecule may fit into this groove and therefore might play a major role in the lipid−protein interaction.

From $^1$H NMR experiments performed on the PMP1 fragment (G13−F38) solubilized in DPC-$d_{38}$ micelles, we have first investigated the influence of the A21L mutation on POPS binding. This mutation was designed to alter the helix groove by substituting a methyl group with a bulky side chain. In a second step, we have carried out POPS titration experiments on the wild-type (WT) peptide, monitored by a full set of one- and two-dimensional NOESY spectra, to directly follow the formation of the phospholipid−PMP1 association and investigate the role of the helix groove. The suitability of these experiments benefits from the ability of $^1$H NMR spectra to distinguish the *sn*-1 and *sn*-2 chains of lipids in micelles (*41*).

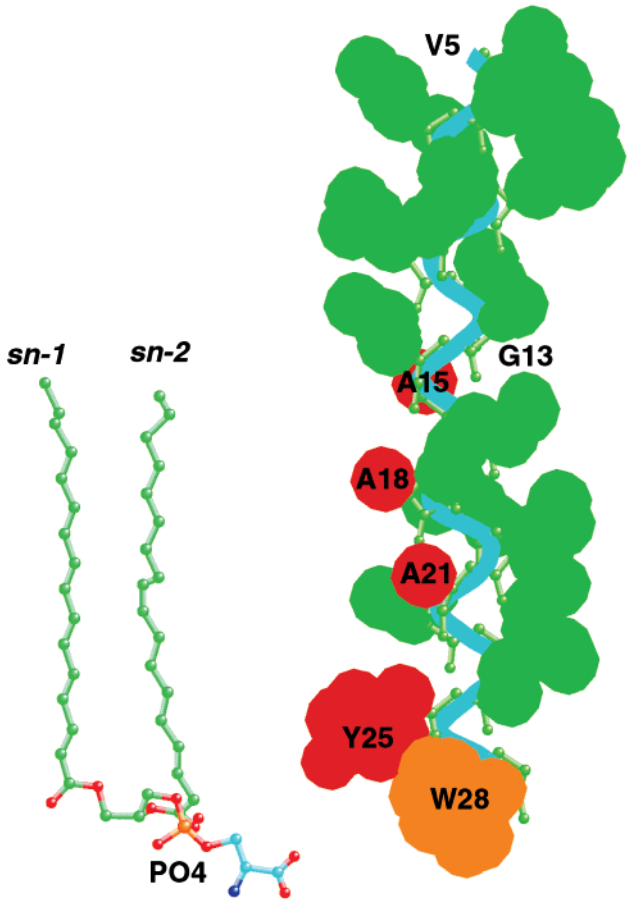


FIGURE 1: Working molecular models of PMP1 (right) and POPS (left). Hydrogen atoms are not shown. On the right, only the V5−W28 sequence of PMP1 is displayed as a helix; the hydrophobic side chain atoms are shown as green spheres, except for the alanine and Y25 side chains colored in red and that of W28 in orange. The R26 and K27 polar side chains are not shown. On the left, the carbons of the *sn*-1 and *sn*-2 acyl chains of POPS are colored in green. Oxygen, phosphate, and nitrogen atoms of POPS are colored red, orange, and blue, respectively; carbon atoms of the serine headgroup are colored cyan. Molecular modeling was performed using Sybyl (Tripos Inc.).

## MATERIALS AND METHODS

*Peptide Synthesis and Purification.* Peptides were synthesized using continuous-flow Fmoc/tBu chemistry (*42*) on an Applied Biosystems (Foster City, CA) Pioneer peptide synthesizer. All chemical reagents were purchased from Applied Biosystems. HATU and DIPEA were used as coupling reagents. Both peptides were blocked at the N-terminus with an acetyl group and at the C-terminus with an amide. The Cys16 residue was substituted with a serine to avoid the oligomerization effect. The syntheses were performed using Fmoc-PAL-PEG-PS resin. Stepwise elongation of the peptide chain was accomplished using the extended double-coupling protocol. Deblock steps were improved with two successive deliveries of piperidine instead of one. N-Terminal acetylation was achieved on the peptide resin at the end of the synthesis with acetic anhydride. A 92.5/2.5/2.5/2.5 (v/v) TFA/water/TIS/EDT mixture was used for cleavage. After removal from the resin and deprotection, the cleavage product was precipitated in cold diethyl ether, then dissolved with a mixture of aqueous TFA buffer and acetonitrile, and lyophilized. Crude peptides were directly purified by reverse-phase medium-pressure liquid chromatography (MPLC) on a Nucleoprep 20 mm C18 100 Å preparative column, using a 35 to 82% linear gradient of acetonitrile in 0.08% aqueous trifluoroacetic acid (TFA) (pH 2) for 60 min at a flow rate of 25 mL/min. The purity of the peptides was verified on a nucleosil 5 mm C18 100 Å analytical column, using a 40 to 60% linear gradient of acetonitrile in 0.08% aqueous TFA (pH 2) for 20 min at a flow rate of 1 mL/min. Purified peptides were then quantified by amino acid analysis and finally characterized by using positive ion electrospray ionization mass spectrometry (ES+). G13−F38 from the wild type: synthesis scale, 0.2 mmol; total yield, 25% (150 mg); mass spectrometry data, 3071.29 ± 0.30 (expected, 3071.70). G13−F38 from

A21L: synthesis scale, 0.1 mmol; total yield, 21% (64 mg); mass spectrometry data, 3113.80 ± 0.29 (expected, 3113.78).

*NMR Experiments.* Samples were prepared using 3 mM PMP1 fragments solubilized in either 90/10 $H_2O/D_2O$ or pure $D_2O$ solutions containing 120 mM DPC-$d_{38}$ micelles (CIL). The pH value was adjusted to 5. $^1$H NMR experiments were carried out on 500 and 800 DRX Bruker spectrometers. Proton chemical shifts (±0.005 ppm) were referenced to an internal standard DSS. The 800 MHz spectra were recorded on the spectrometer installed at ICSN-CNRS (Gif-sur-Yvette, France), procured with the help of the Région Ile de France and the Association pour la Recherche contre le Cancer. For the conformational study of the A21L mutant, 500 MHz TOCSY and NOESY spectra were recorded at 35 °C with mixing times of 80 and 100−250 ms, respectively. POPS titration experiments on the wild-type peptide were performed by adding solid aliquots of POPS (Avanti Polar Lipids) to the peptide samples. The [POPS]/[peptide] ratios were directly measured from spectra obtained in a pure $D_2O$ solution by integrating the signals corresponding, on one hand, to the *sn*-2 CH═CH and glycerol CH protons of POPS and, on the other hand, to the aromatic protons of the peptide (the area surface uncertainty is ±5%). Two independent sets of measurements were performed, attesting to the reproducibility of the titration curves within experimental error. The 500 and 800 MHz one- and two-dimensional NOESY spectra of the samples were recorded at pH 5 and 25 °C. POPS−peptide intermolecular cross-peaks were identified by comparing NOESY spectra recorded in the absence and presence of POPS. Mixing times of 100, 300, and 500 ms were used. For modeling PMP1 and POPS, we used the last release, 6.8, of Sybyl (Tripos Inc.). A Tripos force field with electrostatics was used for minimization.

## RESULTS

*Effect of the A21L Mutation.* The influence of the A21L mutation on the conformational and POPS binding properties of the PMP1 G13−F38 fragment was investigated from standard two-dimensional $^1$H NMR experiments. They were first performed on the A21L mutant solubilized in DPC-$d_{38}$ micelles in the absence of phospholipids. Both NOE and chemical shift data indicate that the A21L mutation induces no structural change on the peptide average conformation (data not shown). The A21L mutant was then cosolubilized in DPC micelles with an amount of POPS corresponding to a [POPS]/[peptide] ratio of ∼4, which satisfies the experimental conditions already used for studying the wild-type (WT) peptide and several mutants (*37*). This model system provides a suitable NMR reporter specific to PMP1−POPS binding, i.e., a shift ($\Delta\delta$) induced on the CH═CH resonance of the lipid *sn*-2 oleoyl chain, which is not observed in the presence of POPC. A mutation effect on POPS binding can thus be readily monitored by measuring this characteristic shift. The $\Delta\delta$ value corresponding to the A21L substitution is compared in Figure 2 to those previously obtained for the wild-type (WT) peptide and the mutants Y25L, W28L, Q29S, and Q32S (*37*). One can observe that the A21L mutation reduces the magnitude of the high-field shift characteristic of POPS−WT peptide binding as much as the Q32S mutation. In other words, a mutation designed for altering the "alanine" groove of the helix disfavors the POPS binding specificity as much as that affecting the electrostatic interaction network. The behavior of the A21L mutant highlights the major role played by the helix groove in the POPS binding interaction network. In a second step, POPS titration experiments were performed on the WT peptide.

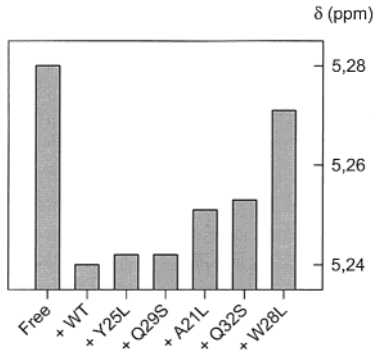


FIGURE 2: Effect of mutation on POPS binding as monitored from the characteristic shift ($\delta$) of the *sn*-2 CH═CH resonance (in parts per million). The first $\delta$ value, labeled free, is observed for POPS in DPC micelles in the absence of peptide. The second value, labeled WT, is observed in the presence of the G13−F38 PMP1 fragment. The following $\delta$ values correspond to various mutants of this fragment (*37*) and include the effect of A21L. All the $\delta$ values were measured at 25 °C and pH 5.

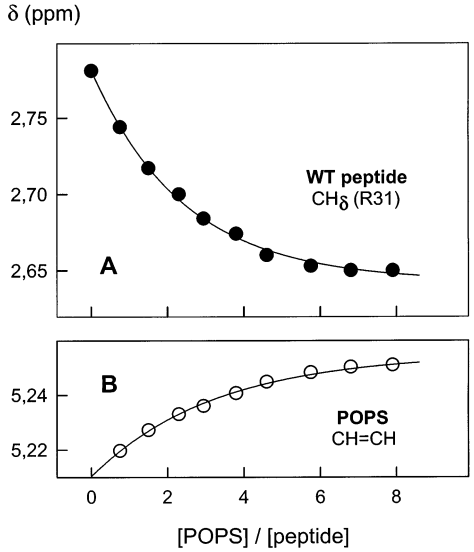


FIGURE 3: POPS titration plots of the chemical shifts that are the most sensitive to POPS binding: (A) the high-field resonance of the R31 C$\delta$H$_2$ group for the PMP1 peptide and (B) the CH═CH resonance of the *sn*-2 POPS chain. The [POPS]/[peptide] ratios were measured as described in Materials and Methods. All the $\delta$ values (in parts per million) were measured at 25 °C and pH 5.

*POPS Titration Experiments Monitored by Chemical Shifts.* The PMP1 G13−F38 fragment was solubilized in perdeuterated DPC micelles in the presence of increasing amounts of protonated POPS. The binding process was first monitored using the most sensitive chemical shift for each partner, i.e., the *sn*-2 CH═CH resonance for POPS, mentioned above, and the high-field resonance of the R31 C$\delta$H$_2$ group for the peptide. Once the phospholipid binds, significant shifts are observed on the polar side chain signals of the PMP1 cytoplasmic domain (*37*) and in particular on those of R31, exhibiting the largest variation in the presence of POPS. The lipid and peptide $\Delta\delta$ values are plotted versus the [POPS]/[peptide] ratio in Figure 3. The curve relative to the R31 proton (Figure 3A) displays a hyperbolic decrease

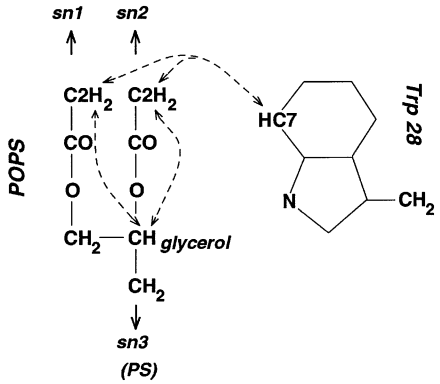


FIGURE 4: Schematic view using dotted lines of (i) the intramolecular POPS NOEs involving, on one hand, the $C2H_2$ protons of the *sn*-1 and *sn*-2 chains and, on the other hand, the CH proton of the glycerol moiety and (ii) the intermolecular PMP1−POPS NOEs involving, on one hand, the $C2H_2$ protons of the *sn*-1 and *sn*-2 chains and, on the other hand, the C7H proton of W28.

with a plateau region reached from a concentration ratio of ~6. In parallel, the CH═CH signal (Figure 3B) undergoes an increasing downfield shift that tends toward a plateau value corresponding to a [POPS]/[peptide] ratio of ~8. Such a number corresponds to the maximum number of POPS molecules covering the contact interface offered by the PMP1 cytoplasmic domain, as judged by a simple computational docking procedure. In agreement with the data obtained in micelles, approximately eight bound POPS molecules were detected from our $^2H$ NMR study of a PMP1 fragment inserted in mixed POPC/POPS bilayers (*40*). The rather exceptional property offered by the PMP1−POPS model in simultaneously monitoring how a specific lipid−peptide interaction network takes place from reporters probing each of the concerned species has to be pointed out.

*POPS Titration Experiments Monitored by Intermolecular NOEs*. As previously shown (*37*), the protons of the aromatic residues (Y25, W28, and F38) of the G13−F38 peptide give rise to NOE cross-peaks with those of POPS, easily detected since they are located far from the overcrowded aliphatic region. Opportunely, the Y25 and W28 side chains border the C-terminal entry site of the alanine groove within the PMP1 helix; when viewed along the helix axis direction, the α-carbon of A21 appears to be located just between those of the Y25 and W28 residues (Figure 1). Furthermore, intermolecular NOEs were observed between the aromatic protons and the first methylene group ($C2H_2$) of both POPS acyl chains, *sn*-1 and *sn*-2, that fortunately correspond to separate signals (*41*). We have therefore analyzed the POPS concentration dependence of these appropriate NOEs, which are able to distinguish the *sn*-1 and *sn*-2 chains. As a control, we have compared their behavior to that of intramolecular NOEs between POPS protons. Hence, the two following sets of NOEs were considered: (i) the intermolecular NOEs involving, on one hand, either the C7H proton of W28 or the C3H/C5H protons of Y25 and, on the other hand, the $C2H_2$ protons of the *sn*-1 and *sn*-2 chains (the selected aromatic protons give rise to the most intense NOEs) and (ii) the intramolecular NOEs involving, on one hand, the $C2H_2$ protons of the *sn*-1 and *sn*-2 chains and, on the other hand, the CH proton of the corresponding glycerol moiety.

These NOEs are schematically illustrated in Figure 4, the C7H proton of W28 featured as the peptide probe. Figure 5

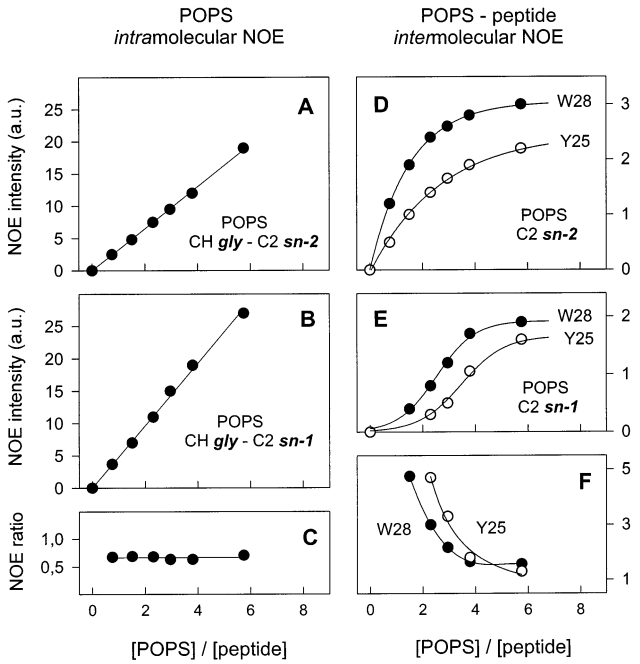


FIGURE 5: POPS titration plots of (A) the intramolecular NOE between the $C2H_2$ protons of the POPS *sn*-2 chain and the CH proton of the glycerol moiety, (B) the intramolecular NOE between the $C2H_2$ protons of the POPS *sn*-1 chain and the CH proton of the glycerol moiety, and (C) the ratio between the two NOEs. POPS titration plots of (D) the intermolecular NOEs between either the C7H proton of W28 (●) or the C3H/C5H protons of Y25 (○) and the $C2H_2$ protons of the POPS *sn*-2 chain, (E) the intermolecular NOEs between either the C7H proton of W28 (●) or the C3H/C5H protons of Y25 (○) and the $C2H_2$ protons of the POPS *sn*-1 chain, and (F) the ratio between the NOE values displayed in panels D and E where the filled and empty symbols correspond to the NOEs involving C7H (W28) and C3H/C5H (Y25), respectively. The [POPS]/[peptide] ratios were measured as described in Materials and Methods.

summarizes the dependence on the [POPS]/[peptide] ratio of the selected intra- and intermolecular NOEs. One can readily observe that these absolute NOE intensities exhibit three distinct behaviors. The intramolecular POPS NOEs display a linear plot (Figure 5A,B), whereas the intermolecular peptide−POPS NOEs reach a plateau value following either a hyperbolic or a sigmoid dependence (Figure 5D,E).

As expected in the absence of conformational change, the intramolecular NOE intensities between POPS protons depend linearly on the concentration of the corresponding species. Therefore, the ratio between the two intramolecular NOEs remains constant with an increase in the POPS concentration (Figure 5C). In the case of the intermolecular NOEs, the curve corresponding to the C7H (W28)−$C2H_2$ (*sn*-2) correlation displays a hyperbolic dependence with 50% of its plateau value reached for a 1/1 [POPS]/[peptide] ratio (Figure 5D, filled symbols). In contrast, the intensity of the C7H (W28)−$C2H_2$ (*sn*-1) NOE represents less than 10% of its plateau value for a 1/1 ratio and follows a sigmoid variation (Figure 5E, filled symbols). To a lesser extent, the same description applies to the NOEs involving the C3H/C5H signal of Y25 (Figure 5D,E, empty symbols).

The dual behavior displayed by the intermolecular NOEs is similar to that observed for spectroscopic parameters monitoring the ligand binding properties of two protein sites that exhibit significantly different affinities (*43*, *44*). To our knowledge, the NOE-based titration plots shown in this report

constitute the first NMR data that directly distinguish the role of the *sn*-1 and *sn*-2 chains in a protein−lipid interaction. As a result of this dual behavior, for a given aromatic proton, the ratio between the intermolecular NOEs relative to the $C2H_2$ (*sn*-2) and $C2H_2$ (*sn*-1) POPS protons dramatically decreases with an increase in the POPS concentration (Figure 5F). In contrast, as mentioned above, the equivalent ratio corresponding to the intramolecular NOEs remains constant (Figure 5C).

At a low POPS concentration, i.e., for approximately one POPS per peptide, the Y25 and W28 side chains that border the C-terminal entry site of the alanine groove are thus essentially sensitive to the presence of the *sn*-2 $C2H_2$ protons. The hyperbolic dependence on the POPS concentration of the corresponding intermolecular NOEs assesses the alanine groove is a high-affinity binding pocket for the POPS *sn*-2 chain. The concerned aromatic protons also display weak NOEs with the glycerol *sn*-2 CH proton and, of course, stronger NOEs with the undifferentiated signals gathering the remaining methylene protons of the POPS chains. The latter give rise to NOEs with the Hα protons of A21 and A18 (data not shown), which further confirms the presence of an acyl chain in the PMP1 helix groove. In contrast, the intermolecular NOEs involving the *sn*-1 protons follow a sigmoid dependence, characterizing a lower-affinity site formed by the external environment surrounding both the Y25 and W28 rings with respect to the alanine groove. As shown by the titration curves, approximately eight POPS molecules are found around the PMP1 cytoplasmic domain when the saturation conditions are reached. Taken together, our data indicate that the clustering of POPS molecules is promoted from a stabilized framework obtained by coupling the PMP1 helix groove to a POPS *sn*-2 chain. Of course, the ring-like interfacial distribution of the five basic side chains (R26, K27, R31, R33, and R37) contributes to the POPS binding around this framework as well as the ability of *one* arginine residue to interact with *two* anionic phospholipids. In addition, the interaction between the POPS headgroups themselves may participate in the overall interaction network triggered by PMP1.

## DISCUSSION

Mutational analysis and NOE titration experiments performed on the G13−F38 fragment of PMP1 demonstrate the formation of a specific POPS−peptide framework in which the *sn*-2 chain fits into the helix alanine groove. The prominence of the *sn*-2 chain over the *sn*-1 chain most probably arises from it being closer to the *sn*-3 moiety comprising the polar head (Figure 4). The *sn*-2 chain insertion is indeed much more appropriate for ensuring an adequate positioning of the PS headgroup with respect to Q32, located just below W28 (Figure 1) and whose influence on the POPS binding specificity has been shown to be essential from our mutational analysis (*37*). As a matter of fact, the PS carboxylate and amino groups can form two complementary H-bonds with a Gln side chain amide. Furthermore, the double bond that impairs the *gauche*−*trans* interconversion in the middle of the *sn*-2 oleoyl chain reduces the entropy cost required for immobilizing the corresponding chain into the groove when compared to a saturated chain such as the *sn*-1 palmitoyl one. Besides, it has to be pointed out that unsaturated acyl chains generally predominate the *sn*-2 position of monounsaturated glycerophospholipids (*45*).

A second point to be discussed is that, whatever the tested experimental conditions, including 800 MHz spectra, the CαH and $C\beta H_2$ protons of the PS headgroup do not display any detectable NOEs with those of the PMP1 cytoplasmic side chains, in particular with Q32. This absence may result from an excessively high flexibility of the related segments with respect to the NOE time scale. It may also be simply due to the upper limit of 5 Å that restricts the detection of NOE effects. Indeed, as readily shown by simple molecular modeling, the H-bonds between the acceptor and donor groups of the PS headgroup and the Q32 side chain correspond to in-plane interactions that maintain the concerned aliphatic protons distant enough to impair any NOE build-up. Despite the lack of direct NOEs, much data strongly support the occurrence of the PS−Q32 interactions: (i) the specific variation of the Q32 side chain chemical shifts observed upon POPS binding (*37*), (ii) the effect of the Q32S mutation already mentioned, and (iii) the essential W28−Q32 side chain−side chain interaction assessed from intramolecular NOEs, which links the Q32 protons to the *sn*-2 $C2H_2$ and glycerol CH protons of POPS through the intermolecular NOEs involving W28, described in this report. These intra- and intermolecular NOEs are fully consistent with an adequate positioning of the Q32 side chain amide with respect to the PS carboxylate and amino groups as well as that of the R31 or R33 side chains with respect to the phosphate group. Using our experimental set of data, a resolved description of the PMP1−POPS association, including the effective dynamic aspects, should be obtained from molecular simulation studies with explicit water and phospholipid molecules, which are in progress in our laboratory.

*Possible Implication for the Role of PMP1 in Its Endogenous Lipid Environment.* In fact, the helix segment of the G13−F38 PMP1 fragment, i.e., G13−Q32, approximately spans a leaflet of a membrane bilayer. The remaining residues of the PMP1 sequence from the N-terminus up to G13 therefore correspond to those exposed to the complementary lipid leaflet. Quite interestingly, from the G3-G4 doublet up to G13, the N-terminal segment of PMP1 exclusively exhibits bulky hydrophobic side chains, which thus contrasts with the alanine groove characterizing the C-terminal segment (Figure 1). The asymmetric distribution of long and short chain hydrophobic residues along the PMP1 helix can also be associated with the absence of polar residues at the N-terminus and the presence of a highly positively charged cytoplasmic domain at the C-terminus.

In turn, these features may be related to the well-known asymmetric distribution of lipids between the outer and inner leaflets of membranes. Such an asymmetry is especially pronounced for the yeast plasma membrane (*34*) in which PMP1 functions as a regulatory subunit of the $H^+$-ATPase. The outer leaflet of this membrane is characterized by a large proportion of sphingolipids and ergosterols, known to favor the formation of rafts, which have been recently detected and include the $H^+$-ATPase (*35*). The inner leaflet contains most of the PS lipids, the prominent species being the monounsaturated POPS, which represents 20% of the total glycerophospholipids. Although no description of the PMP1−ATPase association and, in particular its stoichiometry, is available, our analysis suggests the following functional

scheme. Through their bulky hydrophobic N-terminal segment up to G13, the PMP1 proteolipids might colocalize with the enzyme into the outer sterol−sphingolipid aggregates characterizing the concerned rafts. In that case, each PMP1 C-terminal region may sequester a POPS subset of the inner leaflet through the fine-tuned interaction network described in this work, which modulates the lipid environment surrounding the inner interfacial regions of the $H^+$-ATPase. These regions should be very sensitive to the membrane surface potential and thus to the presence of charged lipids since the enzyme regulates the cytoplasmic pH.

## REFERENCES


1. Doyle, D. A., Cabral, J. M., Pfuetzner, R. A., Kuo, A., Gulbis, J. M., Cohen, S. L., and MacKinnon, R. (1998) *Science 280*, 69−77.
2. Palczewski, K., Kumasaka, T., Hori, T., Behnke, C. A., Motoshima, H., Fox, B. A., Le Trong, I., Teller, D. C., Okada, T., Stenkamp, R. E., Yamamoto, M., and Miyano, M. (2000) *Science 289*, 739−745.
3. Kolbe, M., Besir, H., Essen, L. O., and Oesterhelt, D. (2000) *Science 288*, 1390−1396.
4. Toyoshima, C., Nakasako, M., Nomura, H., and Ogawa, H. (2000) *Nature 405*, 647−655.
5. Fu, D., Libson, A., Miercke, L. J., Weitzman, C., Nollert, P., Krucinski, J., and Stroud, R. M. (2000) *Science 290*, 481−486.
6. Murata, K., Mitsuoka, K., Hirai, T., Walz, T., Agre, P., Heymann, J. B., Engel, A., and Fujiyoshi, Y. (2000) *Nature 407*, 599−605.
7. Gibbons, C., Montgomery, M. G., Leslie, A. G. W., and Walker, J. E. (2000) *Nat. Struct. Biol. 7*, 1055−1061.
8. Zouni, A., Horst-Tobias, W., Kern, J., Fromme, P., Kraub, N., Saenger, W., and Orth, P. (2001) *Nature 409*, 739−743.
9. Dutzler, R., Campbell, E. B., Cadene, M., Chait, B. T., and MacKinnon, R. (2002) *Nature 415*, 287−294.
10. MacKenzie, K. R., Prestegard, J. H., and Engelman, D. M. (1997) *Science 276*, 131−133.
11. Watts, A. (1998) *Biochim. Biophys. Acta 1376*, 297−318.
12. Arora, A., Abildgaard, F., Bushweller, J. H., and Tamm, L. K. (2001) *Nat. Struct. Biol. 8*, 334−338.
13. Fernandez, C., Adeishvili, K., and Wüthrich, K. (2001) *Proc. Natl. Acad. Sci. U.S.A. 98*, 2358−2363.
14. Baleja, J. D. (2001) *Anal. Biochem. 288*, 1−15.
15. Opella, S. J., Ma, C., and Marassi, F. M. (2001) *Methods Enzymol. 339*, 285−313.
16. Arora, A., and Tamm, L. K. (2001) *Curr. Opin. Struct. Biol. 11*, 540−547.
17. Killian, J. A., and Von Heijne, G. (2000) *Trends Biochem. Sci. 25*, 429−434.
18. White, S., and Wimley, W. C. (1999) *Annu. Rev. Biophys. Biomol. Struct. 28*, 319−365.
19. Yuen, C. T. K., Davidson, A. R., and Deber, C. M. (2000) *Biochemistry 39*, 16155−16162.
20. Zhou, F. X., Merianos, H. J., Brunger, A. T., and Engelman, D. M. (2001) *Proc. Natl. Acad. Sci. U.S.A. 98*, 2250−2255.
21. Gratkowski, H., Lear, J. D., and DeGrado, W. F. (2001) *Proc. Natl. Acad. Sci. U.S.A. 98*, 880−885.
22. Therien, A. G., Grant, F. E., and Deber, C. M. (2001) *Nat. Struct. Biol. 8*, 597−601.
23. Fyfe, P. K., McAuley, K. E., Roszak, A. W., Isaacs, N. W., Cogdell, R. J., and Jones, M. R. (2001) *Trends Biochem. Sci. 26*, 106−112.
24. Pebay-Peroula, E., and Rosenbusch, J. P. (2001) *Curr. Opin. Struct. Biol. 11*, 427−432.
25. Simons, K., and Ikonen, E. (1997) *Nature 387*, 569−572.
26. Kurzchalia, T. V., and Parton, R. G. (1999) *Curr. Opin. Cell Biol. 11*, 424−431.
27. Korlach, J., Schwille, P., Webb, W. W., and Feigenson, G. W. (1999) *Proc. Natl. Acad. Sci. U.S.A. 96*, 8461−8466.
28. Brown, D. A., and London, E. (2000) *J. Biol. Chem. 275*, 17221−17224.
29. Radhakrishnan, A., Anderson, T. G., and McConnell, H. M. (2000) *Proc. Natl. Acad. Sci. U.S.A. 97*, 12422−12427.
30. Sprong, H., van der Sluijs, P., and van Meer, G. (2001) *Nat. Rev. Mol. Cell Biol. 2*, 504−513.
31. Edidin, M. (2001) *Trends Cell Biol. 11*, 492−496.
32. Navarre, C., Ghislain, M., Leterme, S., Ferroud, C., Dufour, J.-P., and Goffeau, A. (1992) *J. Biol. Chem. 267*, 6425−6428.
33. Navarre, C., Catty, P., Leterme, S., Dietrich, F., and Goffeau, A. (1994) *J. Biol. Chem. 269*, 21262−21268.
34. Schneiter, R., Brügger, B., Sandhoff, R., Zellnig, G., Leber, A., Lampl, M., Athenstaedt, K., Hrastnik, C., Eder, S., Daum, G., Paltauf, F., Wieland, F. T., and Kohlwein, S. D. (1999) *J. Cell Biol. 146*, 741−754.
35. Bagnat, M., Keränen, S., Shevchenko, A., Shevchenko, A., and Simons, K. (2000) *Proc. Natl. Acad. Sci. U.S.A. 97*, 3254−3259.
36. Beswick, V., Roux, M., Navarre, C., Coïc, Y. M., Huynh-Dinh, T., Goffeau, A., Sanson, A., and Neumann, J. M. (1998) *Biochimie 80*, 451−459.
37. Mousson, F., Beswick, V., Coïc, Y. M., Baleux, F., Huynh-Dinh, T., Sanson, A., and Neumann, J. M. (2001) *Biochemistry 40*, 9993−10000.
38. Mousson, F., Beswick, V., Coïc, Y. M., Huynh-Dinh, T., Sanson, A., and Neumann, J. M. (2001) *FEBS Lett. 505*, 431−435.
39. Beswick, V., Guerois, R., Ochsenbein, F., Coïc, Y. M., Huynh-Dinh, T., Tostain, J., Noël, J. P., Sanson, A., and Neumann, J. M. (1998) *Eur. Biophys. J. 28*, 48−58.
40. Roux, M., Beswick, V., Coïc, Y. M., Huynh-Dinh, T., Sanson, A., and Neumann, J. M. (2000) *Biophys. J. 79*, 2624−2631.
41. Sanson, A., Monck, M. A., and Neumann, J. M. (1995) *Biochemistry 34*, 5938−5944.
42. Chan, W. C., and White, P. D. (2000) *Fmoc Solid-Phase Peptide Synthesis. A Practical Approach*, Oxford University Press, Oxford, U.K.
43. Lundberg, S., Buevich, A. V., Sethson, I., Eflund, U., and Backman, L. (1997) *Biochemistry 36*, 7199−7208.
44. Biekofsky, R. R., Martin, S. R., Browne, J. P., Bayley, P. M., and Feeney, J. (1998) *Biochemistry 37*, 7617−7629.
45. Wagner, S., and Paltauf, F. (1994) *Yeast 10*, 1429−1437.


BI026274B